catalysts

MDPI

Article

Carbon Nitride-Based Catalysts for High Pressure CO_2 Photoreduction

Francesco Conte [1], Elisa I. García-López [2], Giuseppe Marcì [3,*], Claudia L. M. Bianchi [1], Gianguido Ramis [4] and Ilenia Rossetti [1,*]

[1] Chemical Plants and Industrial Chemistry Group, Dipartimento Chimica, Università degli Studi di Milano, CNR-SCITEC and INSTM Unit Milano Via C. Golgi 19, 20133 Milan, Italy
[2] Department of Biological, Chemical and Pharmaceutical Sciences and Technologies (STEBICEF), Università di Palermo, Viale delle Scienze, 90128 Palermo, Italy
[3] "Schiavello-Grillone" Photocatalysis Group, Dipartimento di Ingegneria, Università di Palermo, Viale delle Scienze, 90128 Palermo, Italy
[4] Dipartimento Ingegneria Chimica, Civile ed Ambientale, Università degli Studi di Genova and INSTM Unit Genova, Via all'Opera Pia 15A, 16145 Genoa, Italy
* Correspondence: giuseppe.marci@unipa.it (G.M.); ilenia.rossetti@unimi.it (I.R.); Tel.: +39-091-23737 (G.M.); Fax: +39-02-50314300 (I.R.)

Abstract: In the current research, the productivity of CO_2 photoreduction has been boosted by performing the reaction in an innovative photocatalytic reactor, which allows for operation up to 20 bar. A set of photocatalysts were used, including three types of pristine TiO_2, i.e., one commercially prepared (Evonik P25), one home-prepared by flame spray pyrolysis (FSP), and one obtained by the hydrolysis of $TiCl_4$ (TiO_2exCl), a bare thermo-exfoliated carbon nitride (C_3N_4-TE), and binary materials composed of TiO_2 and C_3N_4-TE. The photoreduction was carried out in water at pH 14 and in the presence of Na_2SO_3 as a hole scavenger. Hydrogen and very small amounts of CO were detected in the head space of the photoreactor, while in the liquid phase, the main product was formic acid, along with traces of methanol and formaldehyde. The composites P25/TE and TiO_2exCl/TE were found to have a higher productivity if compared to its single constituents used alone, probably due to the heterojunction formed by coupling the two materials. Moreover, the high pressure applied in the photoreactor proved to be very effective in boosting the yield of the organic products.

Keywords: CO_2 photoreduction; carbon capture and conversion; photocatalysis; pressurized photoreactor; titanium dioxide; carbon nitride; solar fuels

Citation: Conte, F.; García-López, E.I.; Marcì, G.; Bianchi, C.L.M.; Ramis, G.; Rossetti, I. Carbon Nitride-Based Catalysts for High Pressure CO_2 Photoreduction. *Catalysts* **2022**, *12*, 1628. https://doi.org/10.3390/catal12121628

Academic Editor: Fernando Fresno

Received: 13 November 2022
Accepted: 8 December 2022
Published: 12 December 2022

1. Introduction

Climate change is one of the greatest challenges of the 21st century, influencing almost all aspects of our lives, especially our health [1]. This phenomenon is commonly ascribed to the massive emission of CO_2 into the atmosphere, which is related to every human activity, including energy and goods production, crops, breeding, etc. [2]. It is well known that carbon dioxide is a greenhouse gas which is not impactful as methane or water vapor; however, its average concentration into the atmosphere has risen dramatically since the pre-industrial era, when it was ca. 280 parts per million (ppm), whereas it has now reached a current value of 417 ppm [3]. In order to mitigate the effects of climate change, it is not enough to develop a sustainable worldwide economy, since efficient processes that remove carbon dioxide from the atmosphere are also required to favor this transition, for instance by carbon capture and sequestration (CCS) [4,5], yield boosting [6], or its use as a raw material to be converted into other valuable products through its utilization (CCU) [7]. The latter option is challenging due to the high stability of the CO_2 molecule, but in the last two decades, a significant amount of time and research has been expended attempting to carry out reactions to convert CO_2 under mild conditions [8,9]. Very promising is the reaction

promoted by photocatalysis, in which the CO_2 adsorbed on the surface of a photoactive material (i.e., the photocatalyst) is forced to react with the other adsorbed species through the mediation of photoexcited electrons [10].

Whenever a photocatalyst is illuminated with a light of the proper wavelength, electrons are promoted from the valence band (VB) of this semiconductor to its conduction band (CB), leaving a hole in the former energetic level [10]. Then, the photoexcited electrons can promote reduction reactions that have a more positive potential than the absolute position of the CB, whereas the holes are employed to oxidize the adsorbed species to maintain the electric neutrality [11].

Among a large selection of photoactive materials, TiO_2 has been extensively used as a photocatalyst, usually as anatase, rutile, or a mixture of these, due to its wide availability, chemical inertness, and low toxicity [12]. However, TiO_2 is characterized by a large band gap (BG), which allows the photocatalyzed reactions to occur only when UV light is used, in particular below 365 nm [13]. While this aspect may not be concerning at a lab scale, it surely limits the applicability of titanium dioxide to exploit sunlight, since UV radiation only accounts for ca. 5% of the whole solar spectrum [14]. Furthermore, in photocatalytic processes with a solid photocatalyst, the photogenerated electrons and holes must survive enough to migrate to the photocatalyst surface and react with the adsorbed species. In that regard, the charge recombination rate in titania is quite fast, on the order of the nanoseconds time range, which further limits its activity [15]. Traditionally, the photocatalytic performance of TiO_2 has been improved by surface modification, using either transition metals, such as Pt, Au, and Ag, as well as non-metallic dopants [16–18]. Indeed, the deposition of metallic nanoparticles (NPs) is a well-known method to extend the lifespan of the electron–hole couple because they act as electron sinks (e.g., Pt) [19–22]. Metals can exploit the plasmonic effect and consequently, can provide "hot electrons" to further enhance the activity at a visible wavelength. Tsen et al. [23] reported a high yield of methanol in the photoreduction of CO_2 under UVC using copper-loaded titania. Kaneco [24] used unmodified commercial titanium dioxide (Degussa P25) in a high pressure reactor to perform the conversion of CO_2 to methane. The effect of pressure will be discussed in this paper as well.

On the other hand, the metal-free polymeric catalyst known as graphitic carbon nitride (g-C_3N_4) is gaining attention since it is able to promote photocatalytic reactions such as water splitting and the oxidation of organic substrates while working under sunlight, thanks to its band gap of 2.8 eV, narrower than that of titanium dioxide [25]. It also shares the advantages of the latter, because it can be obtained in large quantities from the direct thermal condensation of inexpensive precursors, mainly melamine, urea, dicyanamide, etc. [26]. C_3N_4 is characterized by a graphitic 2D type structure [27] and, despite its moderate activity due to the high electron/hole recombination rate, the photocatalytic properties can be improved by chemical, mechanical, or thermal exfoliation, so the graphitic-like planes are exposed and functionalized [27]. Calcination is a successful methodology to obtain high surface area C_3N_4 nanosheets (thermal exfoliation, TE). Still, its properties may be tuned via surface modification, or via coupling with other photocatalyst, such as the aforementioned TiO_2, to obtain a composite in which the electronic bands of both these materials are overlapped, so that the photogenerated charges can be better separated [28].

In this work, the CO_2 valorization via photoreduction to both liquid (formic acid) and gaseous products (hydrogen, carbon monoxide, and methane) has been carried out using titanium dioxide-based photocatalysts, such as commercial P25, homemade flame spray pyrolysis (FSP) TiO_2, and titania obtained from the hydrolysis of titanium tetrachloride (TiO_2exCl). A thermally exfoliated carbon nitride (C_3N_4-TE) is also tested as such, and as a composite made by coupling the two semiconductors (P25/TE and TiO_2exCl/TE). The facile synthesis of all these active materials poses the basis for the scale-up to an industrial level. Furthermore, the tests have been carried out using an innovative pilot photoreactor which allows the reaction to work at a high CO_2 pressure of up to 20 bar. This increases the availability of carbon dioxide in the reaction medium, which is water, and

greatly improves the photocatalytic activity of the photocatalyst employed by enhancing the CO_2 surface adsorption over the photocatalyst surface. Photoreactors typically operate at ambient pressure and temperature, due to the need for transparent windows, while in the recent past, we have set up a high pressure photoreactor (up to 20 bar) that also allows for operation at relatively high temperatures in the liquid phase (up to 100 °C). The photoreduction of CO_2 takes advantage of these conditions, expediting mass transfer and kinetics, but most of all, improving the gas solubility and surface adsorption of the reactants. Exceptionally high productivities have been achieved with this assembly, according to the best literature data. The concept was demonstrated by using titania-based samples in our previous experiments, while here we are exploring a new set of materials, never before tested for this application at high pressure, and in principle, extending the visible light harvesting possibilities for this reaction.

2. Results and Discussion

2.1. Characterisation of the Materials

The XRD patterns of all of the catalysts are reported in Figure 1. The XRD patterns of the TiO_2 samples (Figure 1a) evidenced the coexistence of the anatase and rutile polymorphs in all of the samples; the former exhibits a principal reflection at $2\Theta = 25.3°$, while the latter at 27.4° [29]. FSP titania was characterized by slightly higher percentage of the rutile phase, likely due to the higher temperature of the preparation with respect to P25. Moreover, all the TiO_2 samples, except for TiO_2exCl, show high intensity peaks, which are associated with the high crystallinity of the materials. Indeed, TiO_2exCl is mainly composed of the anatase phase, and it lacks long range crystallinity, as evidenced by the broad and low intensity reflections. The two main diffraction peaks for C_3N_4-TE at 13° and 27°, reported in Figure 1b, can be attributed to the (100) and (002) crystallographic planes of the material [27]. As reported in literature, the intensity of the main diffraction peak of C_3N_4 is very low when it is coupled with titania, due to the high crystallinity of P25 [28].

The textural properties (Table 1) indicate that the SSA varied widely among the titania samples. P25 and FSP were prepared with similar flame-based methods and consisted of dense spherical nanoparticles, whose area was mainly due to the external nanoparticle surface. A higher surface area was achieved for TiO_2exCl and for the C_3N_4-TE. TiO_2exCl shows a higher surface area with respect to TiO_2 P25, and this is reflected in the SSA of the composites, although the deposition process leads to a reduction in the surface area.

Table 1. Textural properties and physical-chemical features of the photocatalysts: BET specific surface area (SSA), t-plot micropore volume (V_{tp}), BJH adsorption pore width (W), crystallite size, phases percentage, and band gap values estimated from DR-UV-Vis spectra elaborated as Tauc plots.

Catalyst	SSA [$m^2\ g^{-1}$]	V_{tp} [$cm^3\ g^{-1}$]	W [nm]	Crystallite Size [nm]	Phases [%]	E_{gap} [eV]
TiO_2 P25	47	/	35	A(18); R(27)	A(78); R(22)	3.20
FSP	67	0.02	19.9	A(20); R(25)	A(65); R(35)	3.2
TiO_2exCl	111	/	6.7	/	Poorly crystalline	3.05
C_3N_4-TE	113	0.019	26.8	/	Poorly crystalline	2.80
TiO_2exCl/TE	76	0.036	4.9	/	Poorly crystalline	2.95
P25/TE	39	0.0016	14.1	A(17); R(17)	A(85); R(15)	2.90

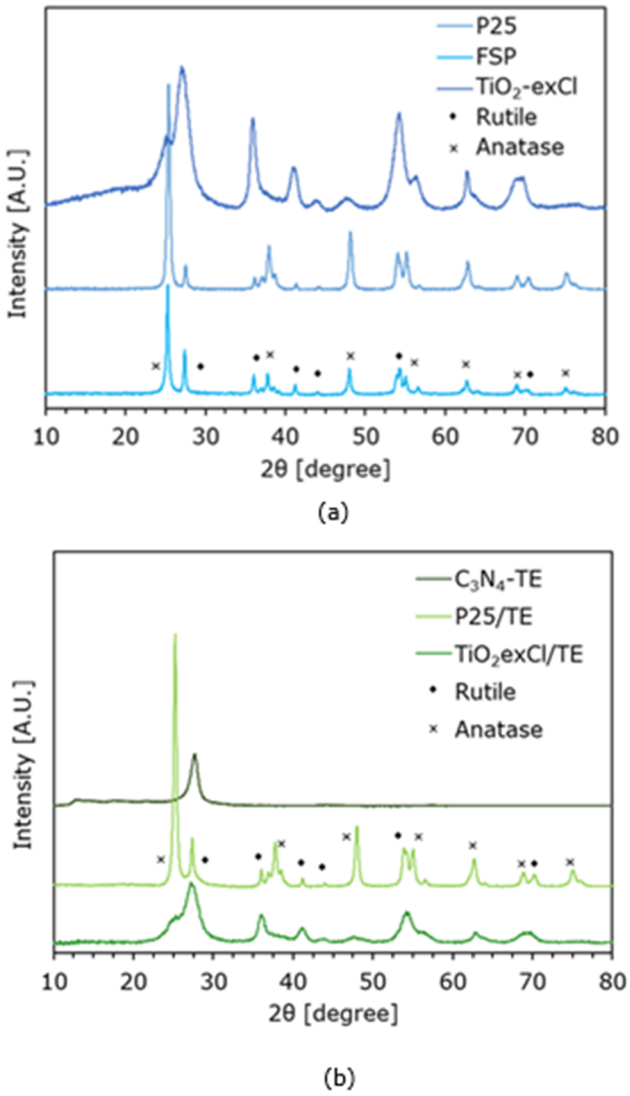

Figure 1. XRD diffractograms of all of (**a**) TiO_2 photocatalysts and (**b**) bare C_3N_4 and TiO_2/C_3N_4 composites. The cross and the square indicate the main reflections of anatase and rutile phases, respectively.

A morphological study of the samples was carried out by scanning electron microscopy (SEM). Figure 2 reports SEM images of TiO_2 FSP, TiO_2exCl, C_3N_4-TE, and the two TiO_2/C_3N_4 composite materials. TiO_2 Evonik P25 SEM pictures are not reported for the sake of brevity, and also because its morphology is well known and reported in previous investigations [30]. The FSP material was comprised of agglomerates of particles, almost spherical, around 20 nm in size. Interestingly, the morphology and the sizes of these particles are very similar to those of TiO_2 Evonik P25. TiO_2exCl appeared to be comprised of agglomerates of particles of almost spherical shape whose size ranged between 100–130 nm. Despite the higher particle sizes of this sample with respect to those of P25, the higher SSA can be attributed to its porosity. The morphology of the C_3N_4-TE material showed the appearance of nanosheets with a thickness of few nanometers, partially twisted on themselves. On the contrary, the morphological aspect of the two composite materials, i.e., P25/TE and TiO_2exCl/TE, were similar to those of the respective bare TiO_2 materials, indicating that titanium dioxide completely covered the carbon nitride surface during the ball milling preparation. However, in the case of TiO_2exCl/TE, some sheets of C_3N_4 were still visible, although they were covered by a film of TiO_2 nanoparticles.

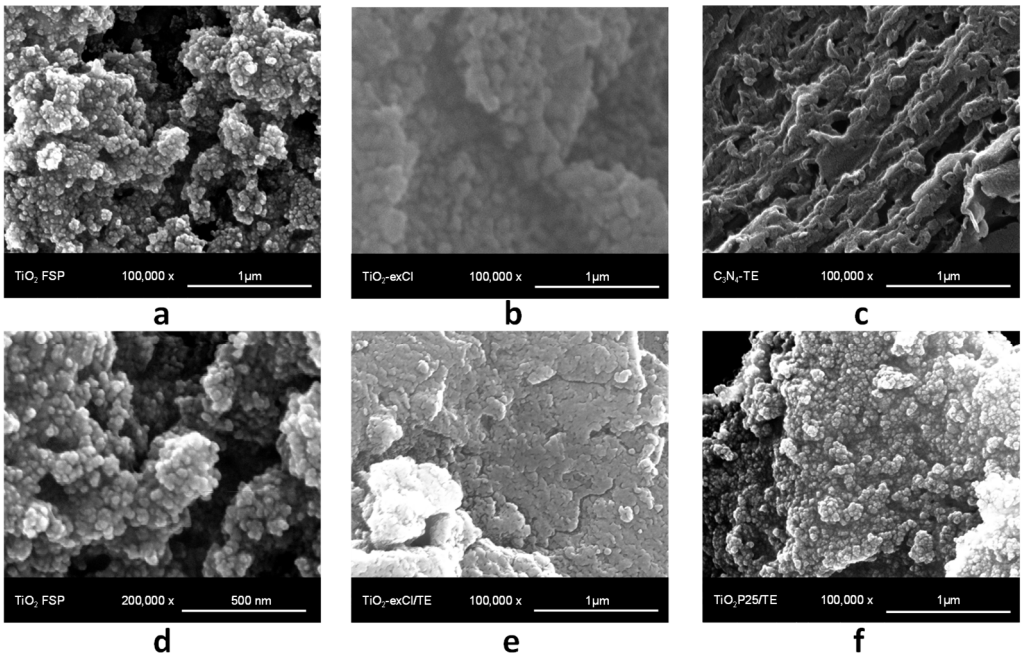

Figure 2. SEM pictures of (**a**,**d**) TiO_2-FSP at different magnifications: (**b**) TiO_2exCl, (**c**) C_3N_4-TE, and both composite materials, (**e**) TiO_2exCl/TE and (**f**) P25/TE.

The FTIR spectrum of the C_3N_4-TE sample (see Figure 3) confirmed the carbon nitride structure, showing the major bands of this structure attributable to the C-N-C and C-NH-C units, i.e., 1632, 1560, 1410, 1325, and 1250 cm^{-1}, typical for the stretching vibration modes of the heptazine heterocyclic ring (C_6N_7) units, as long as the absorption at 887 and 804 cm^{-1} correspond to the N-H deformation mode and a bending mode of the triazine units, respectively [31].

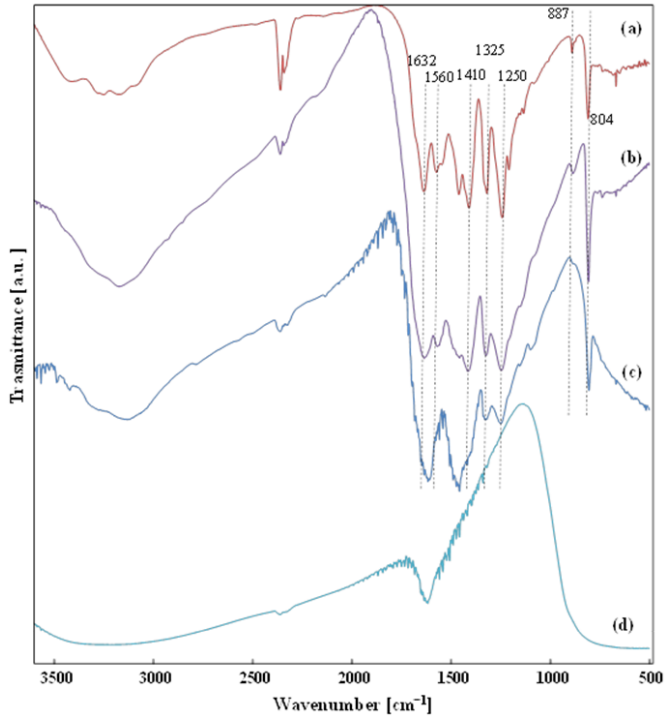

Figure 3. FTIR spectra of (**a**) C_3N_4-TE, (**b**) TiO_2-exCl/TE, (**c**) P25/TE, and (**d**) bare TiO_2-exCl.

Figure 3 also shows a broad band ranging from 3500 to 3000 cm^{-1}, which can be attributed to O-H and N-H stretching, due to the presence of hydroxyl adsorbed species and free amino groups on the surface. The N-H stretching confirms the existence of NH and/or NH_2 groups caused by the incomplete polycondensation of the C_3N_4 [32]. The IR transitions attributed to the heptazine heterocyclic ring are less defined and wider in the composites, indicative of a disorder in the carbon nitride layered structure after the ball milling process in the presence of both titania-containing samples. This is particularly true for the P25/TE sample, for which the SEM micrographs evidenced a uniform coverage of C_3N_4 by the titania nanoparticles. In Figure 3, the FTIR of the bare TiO_2exCl sample is also shown, evidencing the absence of bands in the heptazine range, the presence of water, and the transitions due to the cut-off at ca. 900 cm^{-1} due to the Ti-O-Ti bonds in the oxide sample.

The band gap energy Eg of the catalysts was obtained according to the Tauc equation and the Tauc plots (see Figure 4). The Eg values are reported in Table 1. According to the band gap calculations, the addition of carbon nitride to the P25 has a positive effect on the Eg of the catalyst, lowering its value and extending the absorption of radiation towards the visible range. A similar trend can be observed for TiO_2exCl/TE.

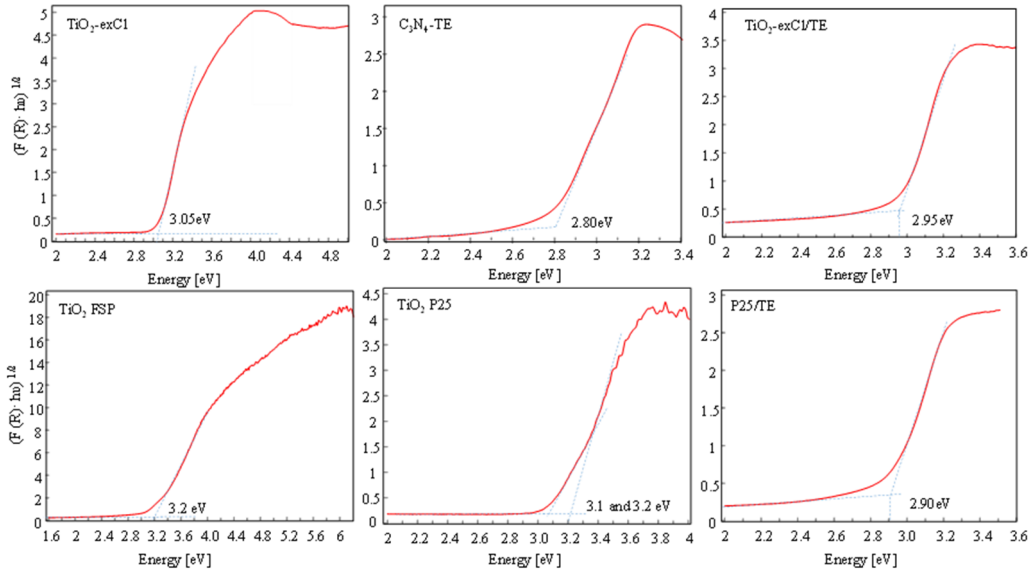

Figure 4. Tauc plots determined from the DR UV-Vis spectra of all the catalysts used.

2.2. Photocatalytic Activity for the Reduction of CO_2

2.2.1. Effect of pH

Photoreduction is a process in which multi-step electron additions are involved and different intermediates are formed, depending on the conditions applied and the photocatalyst used. In addition, the complexity of the mechanism leads to the generation of many products, for instance HCOOH, HCHO, CH_3OH, possible C_2 coupling products, and H_2, CO due to photoreforming. The precise distribution of products and the corresponding productivity vs. operating conditions has been determined in previous works. To summarize, it was observed that the CO_2 conversion increased at basic pH (pH = 14) with respect to a neutral condition. This is justified by the enhanced solubility of carbon dioxide with the formation of both carbonate and bicarbonate in the presence of a base, as TiO_2 is able to adsorb CO_2 and CO_3^{2-} species through either the surface hydroxylic groups (basic) or the coordinated Ti centers on the photocatalyst surface (acidic) [33,34]. On the other hand, DFT calculations pointed out that the adsorption of CO_2 over an ideal plane of carbon nitride mainly occurs via physisorption on the bi-coordinated nitrogen of the triazine/heptazine building blocks [35]; however, real samples of C_3N_4 are characterized by the presence of -NH and -NH_2 moieties on the surface of the sheets, which facilitates the adsorption of

carbon dioxide [25]. Both carbonate and bicarbonate may be reduced to HCOOH and HCHO. In addition, CO_2 solubility further increases with increasing pressure. According to the literature, the back oxidation of formaldehyde to formic acid is favored at basic pH. By contrast, the reduction of formaldehyde to methanol is easier at a lower pH. Our previous research described that the liquid products formed from the photoreduction of CO_2 can further act as hole scavengers with the production of H_2 and CO/CO_2, if the sulfite (hole scavenger, HS) added at the beginning of the reaction is fully consumed. Moreover, the detection of hydrogen can also be the result of direct water splitting promoted by titania, which is quite slow under the selected reaction conditions, as demonstrated by previous blank testing.

The best pH value at which the reaction should be performed may depend on the market demand and value of the compounds formed, as well as their energy storage capacity. We decided to work with a basic pH, as the formic acid, maximized under these conditions, meets both the requirements mentioned above [36,37].

2.2.2. Effect of Pressure

In order to understand effects of pressure on the behavior of the photocatalysts, two sets of tests were performed at 8 and 18 bar of CO_2, and the results are reported in Figure 5. We have selected these two pressure levels as examples of high and intermediate pressure values for comparison with our previous reports. The apparatus allows operation up to 20 bar. High pressure operation typically favors liquid phase products, whereas at intermediate pressure (8 bar), gas evolution may occur, allowing for a better understanding of the behavior of the sample under different regimes.

For the reason described in Section 2.2.1, the pH was increased to 14, and consequently, the obtained formic acid was present in the solution as the formate ion. The catalyst and the HS concentrations were 31 mg/L and 1.67 g/L, respectively. As previously mentioned, the reaction is photocatalytic; indeed, negligible amounts of the products were detected without either the photocatalyst or the UV irradiation. Moreover, the reaction proceeded very slowly when the HS was not added, since the water itself may act as a hole scavenger, but it is well known that its oxidation is kinetically slow.

Overall, the productivity of formic acid and, to a lower extent of H_2, was improved by increasing the pressure. The solubility of CO_2 increases with the applied pressure; therefore, when working at 18 bar, more reactant is available be converted from the reaction medium. Furthermore, increasing pressure also favors the surface adsorption of the reactants over the photocatalyst surface. TiO_2exCl shows the best performance among the three titania photocatalysts tested, with a productivity of formic acid above 7.0 mol/h kgcat at 8 bar, which increases by 64% when a CO_2 pressure of 18 bar is applied. FSP titania seems to benefit the most from the increased pressure, since it increased the productivity by 240% at 18 bar, while the benchmark bare TiO_2 P25 demonstrated a HCOOH productivity increase of 91%, i.e., from 3.2 to 6.2 mol/h kgcat, at the highest pressure. Conversely, the hydrogen evolution did not follow the same trend, except in the case of TiO_2exCl, as its H_2 productivity at high pressure was almost 3.5-fold the value reached at 8 bar. Overall, this is in accordance with the expectations, since it is likely that the hydrogen is evolved mainly when the formic acid itself acts as a hole scavenger, i.e., after the complete conversion of Na_2SO_3, and higher operating pressures should disfavor hydrogen evolution. Formaldehyde and methanol are not reported because negligible amounts were always detected, as expected at this pH [36].

The performance of FSP was similar to that of TiO_2 P25, which is a widely available commercial material. On the contrary, TiO_2exCl showed a significantly higher activity than did the P25 benchmark, deserving some investigation for further improvement. Therefore, the P25 and TiO_2exCl samples were selected for the production of a composite with exfoliated carbon nitride. The top performer of the composite materials was the P25/TE, whose HCOOH productivity reached nearly 14.0 mol/h kgcat, with a 125% increase from the lowest to the highest pressure. The other composite material, TiO_2exCl/TE, and the

bare C_3N_4-TE performed similarly at high pressure, and only slightly better than the titania P25. The HCOOH productivity rose significantly after switching to 18 bar for both of the composite materials.

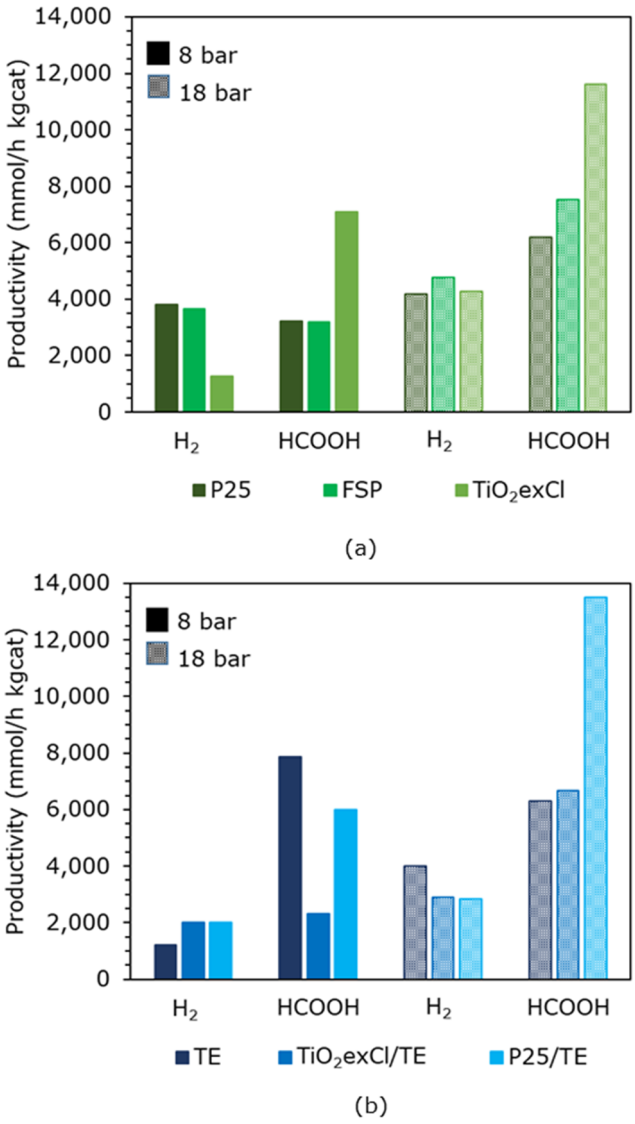

Figure 5. Effect of pressure on product distribution and productivity at 8 and 18 bar with pH = 14, 31 mg/L of catalyst, and 1.67 g/L of HS; reaction time 24 h. (**a**) TiO_2 photocatalysts and (**b**) bare C_3N_4 and TiO_2/C_3N_4 composites. For brevity, the name of C_3N_4-TE sample is here reported as TE.

Overall, the titania from hydrolysis (TiO_2exCl) and the composite P25/TE seemed to be more active than the other materials tested. However, for all the tests carried out, the Na_2SO_3 consumption was close to 100%, and consequently, the HCOOH productivity results were underestimated. Indeed, when Na_2SO_3 disappears from the solution, HCOOH starts to work as HS, and it is oxidized by the hole photoproduced in the VB. This is especially evident for the most active materials. Contemporaneously, the electrons in the CB give rise the reduction of water forming H_2, and therefore, the productivity of H_2 is overestimated.

Consequently, to boost the productivity of formic acid and prevent its consumption in the last stage of the process, after the whole consumption of HS, it was decided to increase the initial concentration of the hole scavenger. Thus, 5.00 g/L of Na_2SO_3 was added to the reactor, and the activity of the two composite catalysts was tested. As reported in Figure 6, along with a drop in the hydrogen productivity, a huge increase in the performance of the

photocatalyst was also observed, with the formic acid productivity rising to 26–31 mol/h kgcat, in the best cases, from a value of 6–14 mol/h kgcat achieved with the standard concentration of HS.

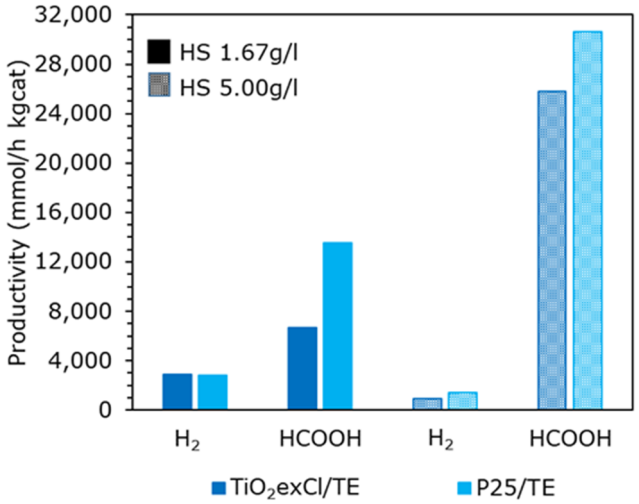

Figure 6. The effect of hole scavenger concentration on product distribution and productivity at 18 bar with pH = 14, 31 mg/L of photocatalyst, and 1.67 g/L or 5.00 g/L of HS concentration; reaction time 24 h.

As expected, the hydrogen production decreased significantly when testing at a high HS concentration, since it mainly comes from the reforming of formic acid, occurring after the consumption of the HS itself. However, despite the 3-fold increase in the HS amount, its conversion was again close to 99%, and, in light of that, we opted for shorter tests, lasting 6 h, using the original HS concentration (1.67 g/L). The results are reported in Figure 7a,b.

At shorter reaction times, even the most active photocatalyst, i.e., P25/TE, did not fully consume the HS (less than 80% conversion), providing significant results regarding the HCOOH productivity. Accordingly, the productivity of gaseous species was very low and was limited to a small amount of H_2, in case of the composite materials, and it was negligible for the other photocatalysts.

The photocatalytic performance can be roughly divided into two groups, since the composites P25/TE, TiO_2exCl/TE, and TiO_2exCl were able to reach HCOOH productivity at around 40 mol/h kgcat; the benchmark P25, FSP titania, and bare TE achieved ca. 16 mol/h kgcat. This is accordance with the conversion of the HS, was around 48% in case of P25, and more than 80% when it was mixed with C_3N_4. Regarding the activity of the photocatalysts based solely on titanium dioxide, TiO_2exCl was clearly the best performer.

Compared to P25 and FSP, the specific superficial area of TiO_2exCl was higher (111 vs. 47 vs. 67 m^2/g), which allows for an increased amount of adsorbed carbon dioxide. In addition, the band gap of the former was 3.05 eV, whereas the other two samples of titania showed an Eg of about 3.2 eV, and a narrower band gap increases the amount of light harvested from a polychromatic light source, such as the medium pressure UV lamp used in this work. On the other hand, the carbon nitride-based composites have band gaps below 3.0 eV; however, both have a lower BET surface area with respect to TE, and they still performed better than the base material.

It has previously been reported that the activity of bare carbon nitride in the photocatalytic reduction of CO_2 is comparable with that of the photocatalysts based solely on titanium dioxide [38–40]. Conversely, when these two materials are coupled and a heterojunction is formed, the C_3N_4 sheets provide the sites for the adsorption of CO_2, while the presence of TiO_2 mitigates the high recombination rate by improving the separation of the charges long enough for the reaction to take place [28,38–40]. In our case, the CO_2

uptake is further improved by the high pressure applied, which leads to the exceptionally high yield of formic acid reported here.

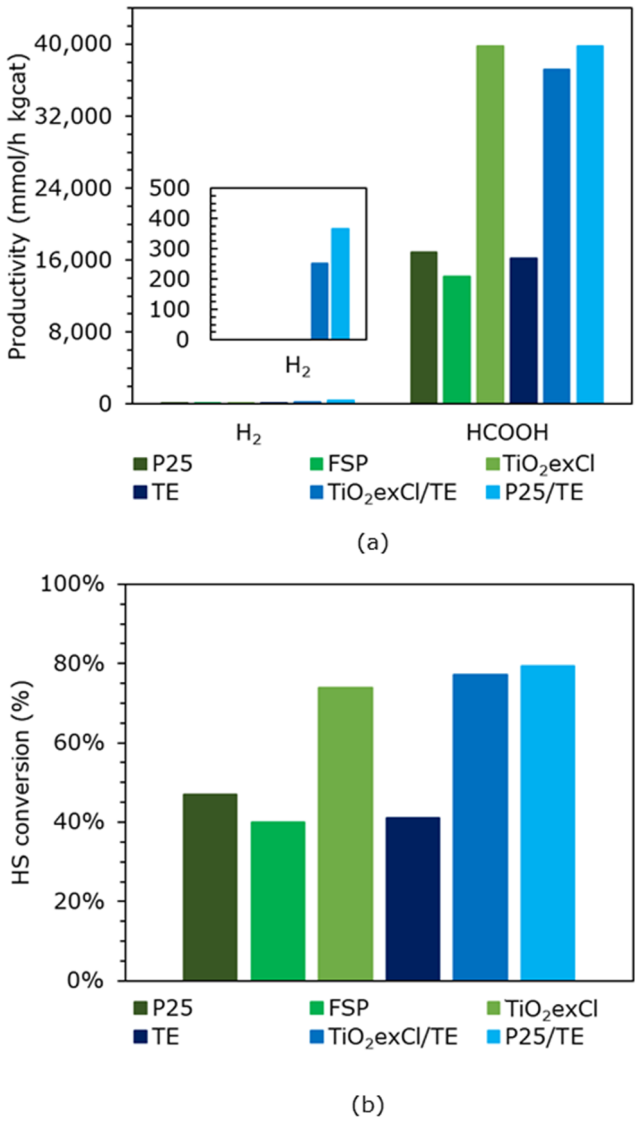

Figure 7. Tests performed at 18 bar, pH = 14, 31 mg/L of photocatalyst, and 1.67 g/L of HS concentration, with a reaction time of 6 h. For brevity, the name of the C_3N_4-TE sample is here reported as TE. (**a**) productivity results and (**b**) hole scavenger consumption.

Furthermore, according to our previous investigations, in the absence of sodium sulphite as a hole scavenger, we did not observe the formation of organic products (from CO_2 photoreduction), nor of hydrogen. When adding the HS, we observed progressive accumulation of CO_2 reduction products over time (only HCOOH at a basic pH, as well as HCHO and CH_3OH at a neutral pH, with lower productivity), and negligible H_2, indicating a faster CO_2 reduction rate than the H_2O reduction rate. When the HS was almost completely consumed, the organic products formed by CO_2 reduction started to act as hole scavengers themselves, with an increasing productivity of H_2 [41]. Therefore, the TiO_2exCl/TE and P25/TE samples are very active, in the sense that they not only formed the highest amount of HCOOH, but they were also able to partially consume HCOOH by photoreforming, with the formation of H_2.

2.3. Energy Efficiency

Finally, in order to make this technology sustainable and competitive, it is necessary to seek for catalysts that efficiently convert the energy from the radiation into chemical bonds, allowing for long-term solar energy storage. This point is crucial, since most of the energy from the renewables (e.g., photovoltaic and wind) is available only for a limited amount of time each day, and availability also varies with the season, the latitude, and the weather conditions at which the plant is located.

In light of this, it is interesting to analyze the efficiency of the energy conversion (from light to chemicals) of the highest performing photocatalyst, such as the composite P25/TE. Its maximum measured formic acid productivity is up to 39.8 mol/h kgcat, which was equal to 9.1 mmol in our batch reactor at the end of the process, or 0.42 g. The higher heating value (HHV) of HCOOH is 5.52 kJ/g, so the overall energy content of the products, without considering the small contribution of H_2, is equal to 2.32 kJ. On the other hand, the UV lamp is powered by a 250 W power supply, and despite the fact that most of the energy is dissipated through heat, that power can be used to assess the energy consumption of our system, which is equal to 5.4 MJ after 6 h of irradiation. Then, the overall efficiency of the process can be calculated according to the following equation (Equation (1)):

$$\text{Energy Efficiency (on lamp power) [\%]} = (E_{HCOOH}\ [J])/(E_{lamp}\ [W] \times \text{time [s]}) \times 100 \quad (1)$$

That calculation results in a 0.04% efficiency in the selected case (P25/TE and the conditions described above), considering lamp consumption (Equation (2)). However, another important performance indicator is the energy efficiency of irradiance (EEI), calculated by referring to the real irradiance, which is lower than the lamp power consumption. This is specifically important to assess the feasibility in the case of natural solar irradiation or other free sources of photons. This efficiency is calculated according to Equation (2), considering a mean irradiated surface around the lamp in the photoreactor, based on reactor geometry.

$$\text{EEI [\%]} = (E_{HCOOH}\ [J])/(E_{irradiance}\ [J\ h^{-1}\ m^{-2}]] \times \text{time [h]} \times \text{mean irradiated surface [m}^2\text{]}) \times 100 \quad (2)$$

In the case of the best performing catalyst used in this work (P25/TE), the calculation of this parameters returns 1.2% efficiency. This is a very impressive result, notwithstanding the small absolute value, with respect to the literature results collected at ambient pressure and temperature [42,43] and those from natural photosynthesis (0.4%); it is attributable to the combination of the high catalytic activity of the selected samples and the very particular high pressure conditions, which are able to boost the productivity.

3. Materials and Methods

3.1. Materials Preparation

The commercial TiO_2 P25 was supplied by Evonik [44], whereas two additional TiO_2 home-prepared materials were obtained using two methodologies.

The TiO_2 nanoparticles were obtained by flame spray pyrolysis (FSP) using a home-developed apparatus described elsewhere [45]. Briefly, titanium isopropoxide (Sigma Aldrich, St. Louis, MO, USA, pur. 97%) was used as the titania precursor, diluted to 0.7 M in a 1:1 *v*/*v* mixture of o-xylene (Sigma Aldrich, 97%) and propionic acid (Sigma Aldrich, 99%). The solution was pumped (2.7 mL min^{-1}) through a capillary tube into a nozzle and dispersed with an oxygen flow (5 L min^{-1}); then, the formed aerosol was ignited by a twelve-hole cone-shaped burner which surrounded the nozzle. The organic solution was co-fed with a mixture of methane and oxygen (0.5 L min^{-1} of CH_4 and 1 L min^{-1} of O_2). The pressure drop at the nozzle was 1.5 bar. The flame produced an instantaneous vaporization of the solution and the pyrolysis of the precursor. The so-formed TiO_2 nanoparticles were deposited in the upper section of the apparatus. Generally, FSP catalysts show a higher surface area and higher thermal stability than solid-state or wet prepared oxides.

The second methodology to prepare TiO_2 was the hydrolysis of $TiCl_4$, as described previously [46]. In brief, titanium tetrachloride (Fluka, St. Louis, MO, USA, pur. 98%) was

added to distilled water ($TiCl_4/H_2O$ 1:10 v/v) at room temperature. After 12 h of stirring, the solution was boiled for 0.5 h under vigorous stirring, obtaining a milky white TiO_2 dispersion that was dried under vacuum at 50 °C to recover the solid labelled as TiO_2exCl.

Bulk graphitic carbon nitride (g-C_3N_4) was prepared by the thermal condensation of melamine, according to the methods in [47]. Melamine (10 g) was placed in a covered ceramic crucible and heated by increasing the temperature by 2 °C min^{-1} up to 520 °C. After maintaining this temperature for 2 h, the oven was slowly cooled down. The resulting yellow powder underwent a successive heating treatment in order to obtain a thermo-exfoliated material showing an increased specific surface area, with respect to the native sample. In particular, the yellow g-C_3N_4 was heated by 3 °C min^{-1} in a static air atmosphere at 520 °C, and maintained for 2 h before cooling down. The resulting pale-yellow powder was labelled as C_3N_4-TE.

Binary materials composed of C_3N_4-TE and TiO_2 P25 or TiO_2exCl were prepared by mechanically mixing both components in a planetary ball mill (Retsch, PM 100 CM, Haan, Germany). For that aim, 2 g of C_3N_4-TE were mixed with 6 g of TiO_2 P25 or TiO_2exCl. The amount of TiO_2, in the case of the composite containing TiO_2 P25, was selected in order to obtain the same surface area of the C_3N_4-TE used (ca. 300 m^2). The mixture was placed in a zirconia jar equipped with zirconia balls of 1 cm diameter. The mixture was rotated at 250 rpm for 1 h inside the planetary mill. The two composites were labelled as P25/TE and TiO_2exCl/TE.

3.2. Physical-Chemical Characterization of the Materials

X-ray diffraction (XRD) analyses were performed using the Rigaku D III-MAX horizontal-scan powder diffractometer (Tokyo, Japan) with Cu-Kα radiation and a graphite monochromator on the diffracted beam.

The N_2 adsorption and desorption isotherms of the samples were measured with a Micromeritics ASAP2020 apparatus (Norcross, GA, USA). The BET SSA (Brunauner-Emmett-Teller Specific Surface Area) and pore volume were calculated from the N_2 adsorption/desorption isotherms, collected at −196 °C, for the samples previously outgassed at 150 °C for 4 h. The micropore volume was calculated according to the t-plot method. BET linearization was used in the range 0.05–0.30 P/P° to calculate the specific surface area (SSA). The Barrett–Joyner–Halenda model (BJH) was used to determine the pore-size distribution from the adsorption branch.

The Diffuse Reflectance (DR) UV-Vis spectra of the samples were recorded on a Shimadzu UV-3600 Plus UV-Vis spectrophotometer (Kyoto, Japan) in the range of 200–800 nm, using an integrating sphere and $BaSO_4$ as the reference standard. The results were processed according to the Kubelka–Munk theory, using Equation (1) to convert the reflectance spectra into the absorption spectra [48].

$$F(R_\infty) = [(1 - R_\infty)]^2/(2\,R_\infty) \quad (3)$$

To obtain the band gap of the samples, the Tauc plots were obtained by plotting the function $(F(R_\infty)\,h\nu)^{1/r}$ (with r = 2 for indirect band gap) versus the energy of irradiation, $h\nu$ [49].

Scanning electron microscopy (SEM) was performed using a FEI Quanta 200 FESEM microscope, operating at 20 kV, on specimens upon which a thin layer of gold had been evaporated. The FTIR spectra of the samples in KBr (Aldrich) pellets were obtained by using a FTIR-8400 Shimadzu (Kyoto, Japan) spectrometer with 4 cm^{-1} resolution and 256 scans.

3.3. Photoreactor and Testing Conditions

All the tests were performed using an innovative pressurized batch photoreactor (Figure 8), whose detailed description has been reported elsewhere [50]. Briefly, it has a cylinder shape and is surrounded by a cooling/heating jacket in which water circulates. The temperature is regulated by a thermostatic system. The reactor is provided with an axial

quartz window which allows for the introduction of a lamp. The apparatus is designed to work under pressure up to 20 bar and with temperatures not higher than 90 °C. The internal volume (with the cap secured) is about 1.3 L, and 1.2 L of liquid was used for each experiment. A magnetic stirrer set at 400 rpm and placed under the reactor ensures the dispersion and mixing of the catalysts.

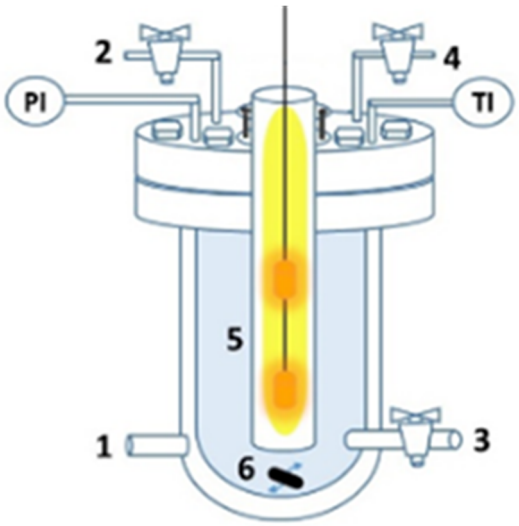

Figure 8. Sketch of the high-pressure photo-reactor, adapted and reproduced from [50]. (1) water colling system (2) gas inlet (3) liquid sampling port (4) gas sampling port/purge (5) quartz sleeve (6) magnetic stir bar.

The photons are supplied by means of a 250 W medium pressure Hg vapor lamp made of two bulbs, which emits in the range of 254–364 nm. The average irradiance during the reported tests was 152.63 W/m^2, as measured in the UVA range by a delta OHM HD 2102.2 photoradiometer. The optimal catalyst and hole scavenger (HS) concentration, investigated in a previous study [36], were 31 mg L^{-1} of photocatalyst and 1.67 g L^{-1} of HS. Each test lasted for 24 h, if not specified differently. The productivity was expressed as mmol/h kgcat, dividing the whole amount of the product produced by the duration of the test.

Na_2SO_3 was used as the inorganic HS, and no products of any type were detected without its addition. The suspension containing both HS and the photocatalyst was saturated overnight with CO_2 at the desired pressure and room temperature. Hence, the resulting pressure is taken as the starting value. The reaction starts when the lamp is switched on and the temperature in the reactor reaches 80 °C (measured with a thermocouple). In order to determine the composition of the reacting suspension, 3 aliquots of 10 mL each are taken at the beginning and at the end of the reaction, and the mixture was centrifuged in order to remove the catalyst.

The liquid samples were analyzed via HPLC (LC-4000 series, Jasco, Tokyo, Japan). The latter was equipped with both UV (UV-4074, Jasco) and refractive index (RI-4030, Jasco) detectors. The column was a 2000-0 BP-OA, Benson Polymeric, and the eluent was an aqueous H_2SO_4 solution (0.5 mmol L^{-1}). Multiple injections of the same sample yielded reproducible results, given that the maximum error of the chromatographic analysis was ca. 5%, and repetition of the same test under identical conditions led to an experimental error of up to 10%.

The residual HS amount in the liquid has been evaluated via iodometric titration. To a precise volume of the sample, excess acid was added (1 M HCl), along with potassium iodide (0.02 M) and the proper amount of potassium iodate solution (0.002 M). Then, the mixture was titrated with sodium thiosulfate (0.002 M) until discoloration occurred.

The gas products were collected in the headspace of the photoreactor and analyzed by a gas chromatograph (Agilent 7890, Palo Alto, CA, USA) equipped with a TCD detector, two columns in series (HPplot Q and HP Molsieves), and a sampling loop of 250 µL. The

timing and valve settings were set for the quantification of H_2, CH_4, and both polar/non-polar light gases. The TCD detector was heated to 200 °C with a helium reference flow of 20 mL/min. During the analysis, the flowrate of helium through the column was equal to 5.5 mL/min, with an overall analysis time of 22 min. The oven temperature was kept at 70 °C for the first 15 min and then increased to 180 °C.

Proper blank tests in the absence of a catalyst, irradiation, or a hole scavenger evidenced negligible product formation. All the activity results have been reported as productivity, i.e., calculating the moles cumulatively obtained for each compound and dividing them by the mass of the catalyst and the time of reaction. The conversion of the hole scavenger is also calculated from the result of the iodometric titration as the converted moles of sulfite divided by the initial amount.

4. Conclusions

The CO_2 photoreduction was studied by operating the reaction under different pressures and investigating the effects of catalyst formulation, as well as with a comparison of the preparation techniques for titania-based photocatalysts (i.e., P25, FSP, and TiO_2 from $TiCl_4$).

It was confirmed that an increased pressure (e.g., from 8 to 18 bar) led to a large boosting of formic acid production, the main product in the selected conditions.

While for prolonged reaction time, the HCOOH is consumed by photoreforming to obtain H_2, which may be desirable for some applications; shorter tests, e.g., 6 h, allowed for a better comparison of the photocatalytic activity of the selected materials. In this context, the FSP titania performed similarly to the benchmark P25, while TiO_2exCl productivity was more than double that of both of the former, and mainly due to its lower band gap and higher SSA. On the other hand, a similar performance was also observed with the composite materials TiO_2exCl/TE and P25/TE, in which the possible formation of a heterojunction between titania and the g-C_3N_4 greatly enhanced the production of formic acid.

Lastly, a quick evaluation of the efficiency of this setup, expressed as the energy stored in the HCOOH with respect to the energy consumed by the lamp, revealed that the efficiency calculated with respect to the effective irradiance was up to 1.2%, one of the highest values reported in the literature.

Author Contributions: Conceptualization, G.R., C.L.M.B., G.M. and I.R.; methodology, F.C., E.I.G.-L., G.R., C.L.M.B., G.M. and I.R.; validation, G.R., C.L.M.B., G.M. and I.R.; formal analysis, G.R., C.L.M.B., G.M. and I.R.; investigation, F.C., E.I.G.-L., G.R. and C.L.M.B.; resources, G.R., G.M. and I.R.; data curation, F.C., E.I.G.-L., G.R., G.M. and I.R.; writing—original draft preparation, F.C., E.I.G.-L., G.R., G.M. and I.R.; writing—review and editing, F.C., E.I.G.-L., G.R., G.M. and I.R.; supervision, G.M. and I.R.; project administration, G.M. and I.R.; funding acquisition, G.R. and I.R. All authors have read and agreed to the published version of the manuscript.

Funding: I. Rossetti and G. Ramis gratefully acknowledge the financial contribution of Fondazione Cariplo through the grant 2021-0855—"SCORE—Solar Energy for Circular CO_2 Photoconversion and Chemicals Regeneration", funded in the frame of the Circular Economy call 2021. I. Rossetti acknowledges Università degli Studi di Milano for support through the grant PSR 2021—GSA—Linea 6, "One Health Action Hub: University Task Force for the Resilience of Territorial Ecosystems".

Data Availability Statement: All the significant data are reported in this paper.

Conflicts of Interest: The authors declare no conflict of interest.

References

1. World Health Organization Cop24. *Special Report Cop24 Special Report Health and Climate*; World Health Organization: Geneva, Switzerland, 2015.
2. Ritchie, J.; Dowlatabadi, H. Defining climate change scenario characteristics with a phase space of cumulative primary energy and carbon intensity. *Environ. Res. Lett.* **2018**, *13*, 024012. [CrossRef]
3. Available online: https://www.co2.earth/daily-co2#:~{}:text=417.04%20ppm&text=Units%20%3D%20parts%20per%20million%20(ppm) (accessed on 10 May 2022).

4. International Energy Agency—IEA. *Storing CO_2 through Enhanced Oil Recovery, Combining EOR with CO_2 Storage (EOR+) for Profit*; International Energy Agency—IEA: Paris, France, 2015.
5. Raza, A.; Gholami, R.; Rezaee, R.; Rasouli, V.; Rabiei, M. Significant aspects of carbon capture and storage–A review. *Petroleum* **2019**, *5*, 335–340. [CrossRef]
6. Kimball, B.A.; Idso, S.B. Increasing atmospheric CO_2: Effects on crop yield, water use and climate. *Agric. Water Manag.* **1983**, *7*, 55–72. [CrossRef]
7. Aresta, M.; Dibenedetto, A.; Angelini, A. Catalysis for the valorization of exhaust carbon: From CO_2 to chemicals, materials, and fuels. technological use of CO_2. *Chem. Rev.* **2014**, *114*, 1709–1742. [CrossRef]
8. Perez, A.C.; Diaz-Perez, M.A.; Serrano-Ruiz, J.C. Electrochemical Reduction of CO_2: Overcoming Chemical Inertness at Ambient Conditions. *Electrochem* **2020**, *1*, 56–59. [CrossRef]
9. Shaya, J.; Srour, H.; Karamé, I. Introductory Chapter: An Outline of Carbon Dioxide Chemistry, Uses and Technology. In *Carbon Dioxide Chemistry, Capture and Oil Recovery*, 1st ed.; Shaya, J., Srour, H., Karamé, I., Eds.; InTech: London, UK, 2018.
10. Tan, H.L.; Abdi, F.F.; Ng, Y.H. Heterogeneous photocatalysts: An overview of classic and modern approaches for optical, electronic, and charge dynamics evaluation. *Chem. Soc. Rev.* **2019**, *48*, 1255–1271. [CrossRef]
11. Xie, S.; Zhang, Q.; Liu, G.; Wang, Y. Photocatalytic and photoelectrocatalytic reduction of CO_2 using heterogeneous catalysts with controlled nanostructures. *Chem. Commun.* **2016**, *52*, 35–59. [CrossRef]
12. Oi, L.E.; Choo, M.Y.; Lee, H.V.; Ong, H.C.; Hamid, S.B.A.; Juan, J.C. Recent advances of titanium dioxide (TiO_2) for green organic synthesis. *RSC Adv.* **2016**, *6*, 108741–108754. [CrossRef]
13. Kang, X.; Liu, S.; Dai, Z.; He, Y.; Song, X.; Tan, Z. Titanium dioxide: From engineering to applications. *Catalysts* **2019**, *9*, 191. [CrossRef]
14. Malato-Rodríguez, S. Solar Detoxification and Disinfection. *Encycl. Energy* **2004**, *5*, 587–596. [CrossRef]
15. Yamada, Y.; Kanemitsu, Y. Determination of electron and hole lifetimes of rutile and anatase TiO_2 single crystals. *Appl. Phys. Lett.* **2012**, *101*, 133907. [CrossRef]
16. Bagheri, S.; Muhd Julkapli, N.; Bee Abd Hamid, S. Titanium dioxide as a catalyst support in heterogeneous catalysis. *Sci. World J.* **2014**, *2014*, 727496. [CrossRef] [PubMed]
17. Zielińska-Jurek, A. Progress, challenge, and perspective of bimetallic TiO_2-based photocatalysts. *J. Nanomater.* **2014**, *2014*, 208920. [CrossRef]
18. Kavitha, R.; Kumar, S.G. Review on bimetallic-deposited TiO_2: Preparation methods, charge carrier transfer pathways and photocatalytic applications. *Chem. Pap.* **2020**, *74*, 717–756. [CrossRef]
19. Debeila, M.A.; Raphulu, M.C.; Mokoena, E.; Avalos, M.; Petranovskii, V.; Coville, N.J.; Scurrell, M.S. The influence of gold on the optical properties of sol-gel derived titania. *Mater. Sci. Eng. A* **2005**, *396*, 70–76. [CrossRef]
20. Rosario, A.V.; Pereira, E.C. The role of Pt addition on the photocatalytic activity of TiO_2 nanoparticles: The limit between doping and metallization. *Appl. Catal. B Environ.* **2014**, *144*, 840–845. [CrossRef]
21. Tasbihi, M.; Kočí, K.; Edelmannová, M.; Troppová, I.; Reli, M.; Schomäcker, R. Pt/TiO_2 photocatalysts deposited on commercial support for photocatalytic reduction of CO_2. *J. Photochem. Photobiol. A Chem.* **2018**, *366*, 72–80. [CrossRef]
22. Liu, Z.; Jia, B.; Zhang, Y.; Haneda, M. Engineering the Metal-Support Interaction on Pt/TiO_2 Catalyst to Boost the H_2-SCR of NO_x. *Ind. Eng. Chem. Res.* **2020**, *59*, 13916–13922. [CrossRef]
23. Tseng, I.H.; Wu, J.C.S.; Chou, H.Y. Effects of sol-gel procedures on the photocatalysis of Cu/TiO_2 in CO_2 photoreduction. *J. Catal.* **2004**, *221*, 432–440. [CrossRef]
24. Kaneco, S.; Shimizu, Y.; Ohta, K.; Mizuno, T. Photocatalytic reduction of high pressure carbon dioxide using TiO_2 powders with a positive hole scavenger. *J. Photochem. Photobiol. A Chem.* **1998**, *115*, 223–226. [CrossRef]
25. Kessler, F.K.; Zheng, Y.; Schwarz, D.; Merschjann, C.; Schnick, W.; Wang, X.; Bojdys, M.J. Functional carbon nitride materials-design strategies for electrochemical devices. *Nat. Rev. Mater.* **2017**, *2*, 17030. [CrossRef]
26. Darkwah, W.K.; Ao, Y. Mini Review on the Structure and Properties (Photocatalysis), and Preparation Techniques of Graphitic Carbon Nitride Nano-Based Particle, and Its Applications. *Nanoscale Res. Lett.* **2018**, *13*, 388. [CrossRef] [PubMed]
27. Praus, P.; Svoboda, L.; Smetana, B. Exfoliated nanosheets of graphitic carbon nitride: Study of structure and morphology. In Proceedings of the NANOCON 2016—Conference Proceedings, 8th International Conference on Nanomaterials—Research and Application, Brno, Czech Republic, 19–21 October 2016; pp. 92–97.
28. Elbanna, O.; Fujitsuka, M.; Majima, T. $G\text{-}C_3N_4/TiO_2$ Mesocrystals Composite for H2 Evolution under Visible-Light Irradiation and Its Charge Carrier Dynamics. *ACS Appl. Mater. Interfaces* **2017**, *9*, 34844–34854. [CrossRef]
29. Leong, K.H.; Gan, B.L.; Ibrahim, S.; Saravanan, P. Synthesis of surface plasmon resonance (SPR) triggered Ag/TiO_2 photocatalyst for degradation of endocrine disturbing compounds. *Appl. Surf. Sci.* **2014**, *319*, 128–135. [CrossRef]
30. Bertolotti, F.; Vivani, A.; Moscheni, D.; Ferri, F.; Cervellino, A.; Masciocchi, N.; Guagliardi, A. Structure, morphology, and faceting of TiO_2 photocatalysts by the debye scattering equation method. The P25 and P90 cases of study. *Nanomaterials* **2020**, *10*, 743. [CrossRef] [PubMed]
31. Niu, P.; Zhang, L.; Liu, G.; Cheng, H.M. Graphene-like carbon nitride nanosheets for improved photocatalytic activities. *Adv. Funct. Mater.* **2012**, *22*, 4763–4770. [CrossRef]

32. García-López, E.I.; Abbasi, Z.; Di Franco, F.; Santamaria, M.; Marcì, G.; Palmisano, L. Selective oxidation of aromatic alcohols in the presence of C_3N_4 photocatalysts derived from the polycondensation of melamine, cyanuric and barbituric acids. *Res. Chem. Intermed.* **2021**, *47*, 131–156. [CrossRef]
33. Cao, Y.; Hu, S.; Yu, M.; Yan, S.; Xu, M. Adsorption and interaction of CO_2 on rutile TiO_2(110) surfaces: A combined UHV-FTIRS and theoretical simulation study. *Phys. Chem. Chem. Phys.* **2015**, *17*, 23994–24000. [CrossRef]
34. He, H.; Zapol, P.; Curtiss, L.A. A theoretical study of CO_2 anions on anatase (101) surface. *J. Phys. Chem. C* **2010**, *114*, 21474–21481. [CrossRef]
35. Zhu, B.; Zhang, L.; Xu, D.; Cheng, B.; Yu, J. Adsorption investigation of CO_2 on g-C_3N_4 surface by DFT calculation. *J. CO_2 Util.* **2017**, *21*, 327–335. [CrossRef]
36. Bahadori, E.; Tripodi, A.; Villa, A.; Pirola, C.; Prati, L.; Ramis, G.; Rossetti, I. High pressure photoreduction of CO_2: Effect of catalyst formulation, hole scavenger addition and operating conditions. *Catalysts* **2018**, *8*, 430. [CrossRef]
37. Bahadori, E.; Tripodi, A.; Villa, A.; Pirola, C.; Prati, L.; Ramis, G.; Dimitratos, N.; Wang, D.; Rossetti, I. High pressure CO_2 photoreduction using Au/TiO_2: Unravelling the effect of co-catalysts and of titania polymorphs. *Catal. Sci. Technol.* **2019**, *9*, 2253–2265. [CrossRef]
38. Crake, A.; Christoforidis, K.C.; Godin, R.; Moss, B.; Kafizas, A.; Zafeiratos, S.; Durrant, J.R.; Petit, C. Titanium dioxide/carbon nitride nanosheet nanocomposites for gas phase CO_2 photoreduction under UV-visible irradiation. *Appl. Catal. B Environ.* **2019**, *242*, 369–378. [CrossRef]
39. Reli, M.; Huo, P.; Šihor, M.; Ambrožová, N.; Troppová, I.; Matějová, L.; Lang, J.; Svoboda, L.; Kuśtrowski, P.; Ritz, M.; et al. Novel TiO_2/C_3N_4 Photocatalysts for Photocatalytic Reduction of CO_2 and for Photocatalytic Decomposition of N_2O. *J. Phys. Chem. A* **2016**, *120*, 8564–8573. [CrossRef]
40. Zhou, S.; Liu, Y.; Li, J.; Wang, Y.; Jiang, G.; Zhao, Z.; Wang, D.; Duan, A.; Liu, J.; Wei, Y. Facile in situ synthesis of graphitic carbon nitride (g-C_3N_4)-N-TiO_2 heterojunction as an efficient photocatalyst for the selective photoreduction of CO_2 to CO. *Appl. Catal. B Environ.* **2014**, *158–159*, 20–29. [CrossRef]
41. Galli, F.; Compagnoni, M.; Vitali, D.; Pirola, C.; Bianchi, C.L.; Villa, A.; Prati, L.; Rossetti, I. CO_2 photoreduction at high pressure to both gas and liquid products over titanium dioxide. *Appl. Catal. B Environ.* **2017**, *200*, 386–391. [CrossRef]
42. Zhang, Z.; Wang, Y.; Cui, G.; Liu, H.; Abanades, S.; Lu, H. Improvement of CO_2 photoreduction efficiency by process intensification. *Catalysts* **2021**, *11*, 912. [CrossRef]
43. Zhu, Z.; Liu, X.; Bao, C.; Zhang, K.; Song, C.; Xuan, Y. How efficient could photocatalytic CO_2 reduction with H_2O into solar fuels be? *Energy Convers. Manag.* **2020**, *222*, 113236. [CrossRef]
44. P25-Evonik. Available online: https://corporate.evonik.com/en/product/PR_52000356?name=AEROXIDE-TiO2-P-25 (accessed on 1 November 2022).
45. Compagnoni, M.; Lasso, J.; Di Michele, A.; Rossetti, I. Flame-pyrolysis-prepared catalysts for the steam reforming of ethanol. *Catal. Sci. Technol.* **2016**, *6*, 6247–6256. [CrossRef]
46. Bellardita, M.; García-López, E.I.; Marcì, G.; Palmisano, L. Photocatalytic formation of H_2 and value-added chemicals in aqueous glucose (Pt)-TiO_2 suspension. *Int. J. Hydrog. Energy* **2016**, *41*, 5934–5947. [CrossRef]
47. Krivtsov, I.; García-López, E.I.; Marcì, G.; Palmisano, L.; Amghouz, Z.; García, J.R.; Ordóñez, S.; Díaz, E. Selective photocatalytic oxidation of 5-hydroxymethyl-2-furfural to 2,5-furandicarboxyaldehyde in aqueous suspension of g-C_3N_4. *Appl. Catal. B Environ.* **2017**, *204*, 430–439. [CrossRef]
48. Makuła, P.; Pacia, M.; Macyk, W. How To Correctly Determine the Band Gap Energy of Modified Semiconductor Photocatalysts Based on UV-Vis Spectra. *J. Phys. Chem. Lett.* **2018**, *9*, 6814–6817. [CrossRef] [PubMed]
49. Tauc, J.; Grigorovici, R.; Vancu, A. Optical Properties and Electronic Structure of Amorphous Germanium. *Phys. Status Solidi* **1966**, *15*, 627–637. [CrossRef]
50. Ramis, G.; Bahadori, E.; Rossetti, I. Photoreactors design for hydrogen production. *Chem. Eng. Trans.* **2019**, *74*, 481–486. [CrossRef]